MOLECULAR AND CELLULAR BIOLOGY, May 2007, p. 3313–3326 Vol. 27, No. 9
0270-7306/07/$08.00+0 doi:10.1128/MCB.01476-06

Integrin α1β1 Controls Reactive Oxygen Species Synthesis by Negatively Regulating Epidermal Growth Factor Receptor-Mediated Rac Activation▽

Xiwu Chen,[1] Tristin D. Abair,[1,2] Maria R. Ibanez,[1] Yan Su,[1] Mark R. Frey,[4] Rebecca S. Dise,[3,4] D. Brent Polk,[3,4] Amar B. Singh,[1] Raymond C. Harris,[1,3,5] Roy Zent,[1,2,3,5] and Ambra Pozzi[1,2,5]*

Division of Nephrology, Department of Medicine,[1] and Departments of Cancer Biology,[2] Cell Biology,[3] and Pediatrics,[4] Vanderbilt University Medical Center, Nashville, Tennessee 37232, and Department of Experimental Medicine, Veterans Affairs Hospital, Nashville, Tennessee 37232[5]

Received 9 August 2006/Returned for modification 14 November 2006/Accepted 21 February 2007

Integrins control many cell functions, including generation of reactive oxygen species (ROS) and regulation of collagen synthesis. Mesangial cells, found in the glomerulus of the kidney, are able to produce large amounts of ROS via the NADPH oxidase. We previously demonstrated that integrin α1-null mice develop worse fibrosis than wild-type mice following glomerular injury and this is due, in part, to excessive ROS production by α1-null mesangial cells. In the present studies, we describe the mechanism whereby integrin α1-null mesangial cells produce excessive ROS. Integrin α1-null mesangial cells have constitutively increased basal levels of activated Rac1, which result in its increased translocation to the cell membrane, excessive ROS production, and consequent collagen IV deposition. Basal Rac1 activation is a direct consequence of ligand-independent increased epidermal growth factor receptor (EGFR) phosphorylation in α1-null mesangial cells. Thus, our study demonstrates that integrin α1β1-EGFR cross talk is a key step in negatively regulating Rac1 activation, ROS production, and excessive collagen synthesis, which is a hallmark of diseases characterized by irreversible fibrosis.

Integrin α1β1, a major collagen binding receptor, is expressed in different cell types, including fibroblasts (45), endothelial cells (8), and mesangial cells in the glomerulus of the kidney (30, 53). Integrin α1β1 confers the ability of cells to bind to collagenous substrata, including collagens I and IV (4, 45), and to proliferate on these substrata (45). Moreover, cells expressing integrin α1β1 sense extracellular levels of collagen and downregulate its synthesis at both transcriptional and translational levels (4, 14). Finally, we demonstrated that integrin α1β1 also downregulates the production of reactive oxygen species (ROS) (4, 58).

Following renal injury, mice lacking integrin α1β1 develop more extensive glomerular fibrosis characterized by excessive accumulation of collagen type IV compared to wild-type (WT) mice (4, 58). Increased fibrosis is due to both a direct effect of the lack of integrin α1β1-mediated downregulation of collagen IV synthesis and excessive ROS production by α1-null mesangial cells.

Constitutive production of ROS by mesangial cells, a major cell type found in the glomerulus of the kidney, originates from an intrinsic NADPH oxidase (26, 48) that normally functions at a low level and increases in response to inflammatory stimuli, high glucose, or stress (25, 34, 35, 37, 55). The NADPH oxidase, highly characterized in phagocytes, is a multicomponent enzyme complex that consists of the membrane-bound cytochrome b_{558} ($p22^{phox}$ and $gp91^{phox}$) and cytoplasmic proteins ($p40^{phox}$, $p47^{phox}$, $p67^{phox}$) that translocate to the membrane following cellular stimulation to produce superoxide (3, 9, 47). A multicomponent phagocyte-like NADPH oxidase is also a major source of ROS in many nonphagocytic cells, including mesangial cells. In the phagocyte-like NADPH oxidase, the catalytic subunits are termed Nox proteins, with Nox4 (homologous to $gp91^{phox}$/Nox2) highly expressed in mesangial cells (16, 19, 48). In addition, membrane-bound and cytoplasmic subunits $p22^{phox}$, $p47^{phox}$, and $p67^{phox}$ have also been found in mesangial cells (1, 32, 40, 55) and their expression or membrane assembly is increased following stimulation with angiotensin II, hormones, and high glucose (1, 40, 55). Moreover, the finding that treatment of mesangial cells with antisense against Nox4, $p22^{phox}$, or $p47^{phox}$ prevents angiotensin II- or high-glucose-mediated ROS production (1, 19, 32, 55) clearly demonstrates a role for these NADPH subunits in ROS synthesis by mesangial cells.

One of the major adapters proposed to aid in the interaction of the cytoplasmic subunit $p67^{phox}$ with membrane-bound cytochrome b_{558} is the small G protein Rac (reviewed in references 2, 3, and 22). Within the Rac family, three major members have been described, namely, Rac1, Rac2, and Rac3. Rac1 is ubiquitously expressed, Rac2 is primarily expressed by cells of the hematopoietic lineage (20, 28), while Rac3 is expressed primarily in the brain, nervous system, and mammary gland (6, 36). Rac members are known to be key regulators of the actin cytoskeleton, as well as of the NADPH oxidase system, particularly Rac1 and Rac2 (3, 22). In this context, Rac1 regulates gene expression, cell cycle progression, cell spreading, rearrangement of the actin cytoskeleton, and activation of the nonphagocytic NADPH (22), while Rac2, besides controlling actin-mediated functions, is necessary for activation of phagocytic NADPH oxidase (3, 18). The recent observation that

* Corresponding author. Mailing address: Medical Center North, B3109, Department of Medicine, Division of Nephrology, Vanderbilt University, Nashville, TN 37232. Phone: (615) 322-4637. Fax: (615) 322-4690. E-mail: ambra.pozzi@vanderbilt.edu.

▽ Published ahead of print on 5 March 2007.

fibroblasts lacking Rac1 upregulate Rac3 activation and cellular ROS suggests a potential role for this Rac family member in ROS synthesis (7). Mesangial cells express Rac1 (19, 33), and this small GTPase is required for regulating angiotensin II-dependent ROS production (19), clearly suggesting that Rac1 can control ROS generation in this glomerular cell type.

Integrins have been shown to control cytosolic, as well as mitochondrial, ROS production via interactions with small G proteins. In this context, activation of integrin α5β1 leads to a transient activation of Rac1, followed by mitochondrial ROS production and consequent matrix metalloproteinase synthesis (27, 54). In addition, activation of integrin α2β1 induces NADPH oxidase-mediated ROS production in a p38-dependent manner (21). In contrast to this finding, adherent leukocytes transiently suppress NADPH oxidase activity and ROS production (59). This effect is due to integrin-mediated inhibition of Rac2 as a result of enhanced tyrosine phosphatase activity and decreased Vav1 activation (59). All together, these data clearly suggest that integrin activation can either enhance or inhibit ROS production and this effect is cell and tissue specific.

In the present study, we investigated the mechanisms whereby integrin α1β1 modulates the production of ROS by the NADPH oxidase in order to understand why α1-null mesangial cells produce excessive collagen IV. We show that lack of integrin α1β1 results in constitutively upregulated Rac1 activity due to increased phosphorylation of the epidermal growth factor (EGF) receptor (EGFR) and consequent activation of Vav2, a guanine nucleotide exchange factor (GEF) for the Rho/Rac family of small G proteins. Activated Rac1 is translocated to the cell membrane, resulting in excessive ROS production and consequent excessive synthesis of collagen IV. These findings show that α1β1-EGFR cross talk plays a key role in modulating ROS production and subsequent collagen synthesis, which has critical implications for understanding regulation of the fibrotic response following injury.

MATERIALS AND METHODS

Cell culture. Mesangial cells were isolated from WT and integrin α1-null mice crossed onto the immorto mouse background (gift of D. Cosgrove) as previously described (4) and propagated at 33°C in the presence of 100 IU/ml gamma interferon. For experiments, cells were cultured at 37°C without gamma interferon for at least 4 days before use, as this is the optimal time for immorto mesangial cells to acquire a phenotype similar to that of freshly isolated primary mesangial cells.

Cell transfection. Mesangial cells were transfected with plasmid pEGFP-CL, pEGFP-CL-Rac-N17, or pEGFP-CL-RacL61 by using FuGENE 6 Transfection Reagent (Roche), and flow cytometry was used to select populations of L61Rac- or N17Rac-green fluorescent protein (GFP)-positive cells. Levels of total Rac and GFP-Rac fusion proteins were confirmed by Western blotting with anti-mouse Rac1 antibody.

The retrovirus LZRS-GFP vector, which allows bicistronic expression of the protein of interest and GFP (see reference 43), was used to generate α1KO cell populations reexpressing the full-length human integrin α1 subunit (gift of E. Marcantonio). Stable cell populations expressing high levels of GFP or GFP and the full-length integrin α1 subunit (α1KO-Rec) were selected by flow cytometry with an antibody to the extracellular domain (Calbiochem). Polyclonal cell populations were used in order to avoid some of the pitfalls associated with isolation of monoclonal cell lines.

Immunofluorescence. To visualize actin, Rac1, EGFR, and focal adhesions, serum-starved mesangial cells were plated in serum-free medium on chamber slides precoated with 10 μg/ml collagen IV or fibronectin. After 3 h, cells were fixed in 4% formaldehyde for 10 min and permeabilized with 0.1% Triton X-100 in phosphate-buffered saline (PBS) for 5 min. After blocking with 3% bovine serum albumin (BSA) in PBS, cells were incubated with rhodamine-phalloidin (1:2,000; Molecular Probes Inc.), anti-mouse Rac1 (1:300; Transduction Laboratories), antivinculin (1:100; Upstate Biotechnology), or anti-mouse EGFR (1:200; Upstate) antibodies, followed by the appropriate rhodamine isothiocyanate (RITC)- or fluorescein isothiocyanate-conjugated secondary antibodies (Calbiochem). Slides were mounted with antifade mounting medium (VECTASTAIN; Vector Labs) and analyzed under an epifluorescence microscope (Nikon).

To visualize collagen IV deposition, 10^4 cells were plated on uncoated chamber slides in complete medium. After 3 days, cells were permeabilized in cold acetone for 10 min and blocked with 3% BSA in PBS. Cells were then incubated with anti-mouse collagen IV antibody (1:200 dilution; BD Transduction Laboratories), followed by incubation with RITC-conjugated secondary antibody (1:200 dilution). Collagen IV was quantified as follows. Collagen-positive structures (i.e., RITC-positive images) were imaged, and the color images were converted to black-and-white pictures with Photoshop (Adobe) and processed with the Scion Image program as previously described (44). Collagen IV was expressed as a percentage of the area occupied by collagen IV-positive structures per microscopic field. Six images per cell type were imaged per experiment, with a total of 24 images analyzed.

In some experiments, cells were serum starved for 24 h with or without Na orthovanadate (25 μM; Sigma), genistein (20 μM; Sigma), or the EGFR-specific inhibitor AG1478 (300 nM; Calbiochem) and then plated on collagen IV with or without the reagents indicated above or with human EGF (100 ng/ml; Calbiochem). After 3 h, the cells were processed as described above.

PAK1-PBD pull-down assays. PAK1-p21Rac binding domain (PBD)-conjugated glutathione Sepharose beads were prepared and used as previously described (17). Cells serum starved for 24 h were scraped in 1ysis buffer containing 50 mM Tris-HCl (pH 7.5), 10 mM $MgCl_2$, 200 mM NaCl, 1% NP-40, 5% glycerol, 0.05% Tween 20, 1 mM NaF, 1 mM Na_3VO_4, and proteinase inhibitor (Roche). Eight hundred micrograms of cell lysate was incubated with 30 μl of PAK1-PBD-conjugated glutathione Sepharose beads at 4°C for 1 h. Beads were then centrifuged, washed with 25 mM Tris-HCl (pH 7.6)–30 mM $MgCl_2$–40 mM NaCl–1 mM dithiothreitol–1% NP-40, suspended in 20 μl of Laemmli's sample buffer, boiled for 5 min, and analyzed by Western blotting as indicated below.

Western blot analysis. Beads were subjected to 12% sodium dodecyl sulfate-polyacrylamide gel electrophoresis, and the fractionated proteins were transferred to nitrocellulose membrane and incubated with anti-Rac1 antibody (1:3,000). Immunoreactive proteins were visualized with an appropriate peroxidase-conjugated secondary antibody and an ECL kit. Equal loading was confirmed by analyzing the levels of total Rac1 in 40 μg of total cell lysate.

To detect levels of phosphotyrosine proteins or phosphorylated EGFR, mesangial cells were serum starved for 24 h with or without the antioxidants TEMPOL (5 μM) and diphenyleneiodium (0.5 μM), as previously described (4). Equal amount of cell lysate (40 μg/lane) were analyzed by Western blotting with anti-phosphotyrosine PY-99 antibody (1:1,000; Santa Cruz), anti-phospho-EGFR pY1173 antibody (1:1,000; Santa Cruz), or anti-EGFR antibody (1:200; Upstate).

To detect the levels of total, as well as phosphorylated, Vav2, mesangial cells were serum starved for 24 h with or without AG1478 (300 nM) and equal amounts of cell lysate (40 μg/lane) were analyzed by Western blotting with rabbit anti-p-Vav2 (Tyr-172; 1:1,000; Santa Cruz) and rabbit anti-Vav2 antibodies (1:1,000; Santa Cruz). Anti-Tyr-172 Vav2 antibodies were used since EGFR phosphorylates Vav2 at its N-terminal domain, specifically, Tyr-142, Tyr-159, and Tyr-172 (51).

For collagen IV analysis, cells cultured for 3 days in complete medium were scraped and suspended in 50 mM HEPES (pH 7.5)–150 mM NaCl–1% Triton X-100. Cell lysates (40 μg/lane) were fractionated by 8% sodium dodecyl sulfate-polyacrylamide gel electrophoresis, and the levels of collagen IV were detected with rabbit anti-collagen IV antibody (1:1,000).

Subcellular fractionation of mesangial cells was performed as previously described (57). Equal amounts of cytosol and membrane fractions (40 μg/lane) were analyzed by Western blotting for levels of total Rac, total EGFR, or phosphorylated EGFR with the antibodies indicated above. Anti-N-cadherin (1:1,000; Santa-Cruz) and anti-ERK (1:1,000; Cell Signaling) antibodies were used to validate the purity of the subcellular fractionation products.

Inhibition of TCPTP expression by siRNA. The murine T-cell protein tyrosine phosphatase–non-receptor-type protein tyrosine phosphatase 2 (TCPTP) sequences 5′-GCAGTTGTCATGCTAAACC-3′ and 5′-CGAGAACCATATCTC ACTT-3′ were targeted for RNA interference. Double-stranded small interfering RNAs (siRNAs) were obtained from Ambion. Subconfluent populations of mesangial cells were transfected with a mixture of the two TCPTP siRNAs (15 nM each) or glyceraldehyde-3-phosphate dehydrogenase siRNA (30 nM) as a control with the Effectene transfection reagent (QIAGEN). After 72 h, cells were serum starved for 24 h and equal amounts of cell lysates (40 μg/lane) were analyzed by Western blotting for levels of phosphorylated and total EGFR, as

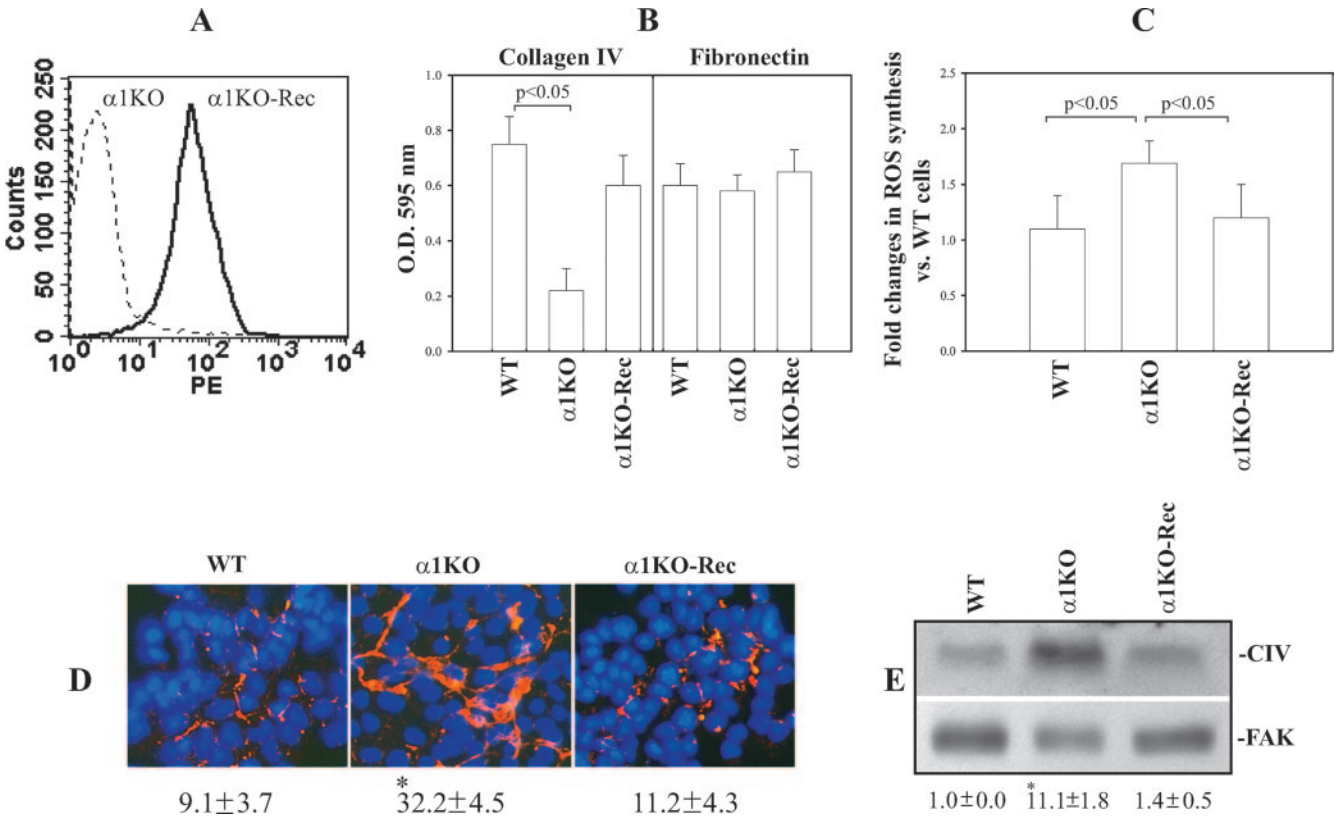

FIG. 1. Integrin α1KO mesangial cells transfected with the integrin α1 subunit downregulate ROS and collagen synthesis. (A) Mesangial cells were transfected with either the empty vector (α1KO) or the human integrin α1 subunit cDNA (α1KO-Rec), and cell populations expressing the integrin α1 subunit were sorted by FACS. PE, phycoerythrin. (B) WT, α1KO, and α1KO-Rec mesangial cells were plated in serum-free medium onto collagen IV or fibronectin (10 μg/ml each) and incubated for 1 h, and their adhesion was determined as described in Materials and Methods. Values represent the mean ± standard deviation of three independent experiments performed in quadruplicate. (C) Mesangial cells (15×10^4 cells/well) were plated on uncoated six-well plates in DMEM containing1% FCS. After 2 days, 2 μM dihydrorhodamine was added and ROS generation was evaluated as described in Materials and Methods. Values are as in panel B. (D) Mesangial cells were cultured on uncoated dishes for 72 h in complete medium, and an indirect immunofluorescence assay was performed to evaluate collagen IV deposition. The percentage of the area occupied by collagen IV-positive structures per microscopic field was quantified with the Scion Image program as described in Materials and Methods. Values are the mean ± standard deviation of four independent experiments. An asterisk indicates a significant difference ($P < 0.05$) between WT and α1KO cells. (E) Lysates (40 μg/lane) from mesangial cells cultured as described for panel D were analyzed by Western blotting for levels of collagen IV (CIV). Membranes were reincubated with anti-FAK antibody to verify equal loading. Collagen IV and FAK bands were quantified by densitometry analysis, and the collagen IV signal is expressed as the collagen IV/FAK ratio. Values are the mean ± standard deviation of three experiments and represent changes (*n*-fold) relative to WT cells. An asterisk indicates a significant difference ($P < 0.05$) between WT and α1KO cells.

well as total TCPTP. Anti-mouse TCPTP antibodies (clone 3E2) were a generous gift of M. Tremblay, McGill University, Montreal, Quebec, Canada (24).

Activation of EGFR in A431 cells. Mesangial cells (2×10^5) were plated onto six-well plates in complete medium. After 12 h, the cells were incubated with 1 ml serum-free medium for 72 h. The medium was collected, and the cells were counted to verify the same number in each well. A431 cells serum starved for 24 h were kept untreated, incubated for 10 min with 1 ml mesangial-cell-conditioned medium, or incubated with 10 ng/ml recombinant EGF. Equal amounts of total cell lysates (5 μg/lane) were then processed for Western blot analysis with anti-pY1173 (1:1,000), anti-phospho-ERK (1:1,000; Cell Signaling), or anti-ERK (1:1,000) antibodies.

ELISA. To determine whether mesangial cells secrete detectable levels of EGFR ligands, 1×10^6 cells were plated on uncoated 10-cm dishes and after 24 h the cells were incubated with 10 ml serum-free medium. At 72 h later, the medium was collected and concentrated to a final volume of 500 μl with Centricon centrifugal filter devices (5,000-Da cutoff) and 100 μl was used to analyze the levels of secreted EGF, HB-EGF, and transforming growth factor alpha (TGF-α) by enzyme-linked immunosorbent assay (ELISA). Briefly, concentrated media were mixed with sodium bicarbonate coating buffer (pH 9.6) to a final bicarbonate concentration of 50 mM and plated in quadruplicate in 96-well Immulon plates (Dynex) under ventilation until dry. Plates were blocked with 2% BSA in PBS for 1 h at room temperature and then probed with antibodies specific for EGF, HB-EGF, and TGF-α (2 μg/ml in 1% BSA in PBS). Anti-TGF-α and -HB-EGF antibodies were from R&D Systems, while the anti-EGF serum was a gift from Stan Cohen. After 1 h, plates were washed with PBS–0.05% Tween 20 and probed with secondary antibodies conjugated to alkaline phosphatase (1:1,000 in PBS–0.05% Tween 20). After 1 h, plates were washed as described above and then exposed to *p*-nitrophenylphosphate substrate (Sigma). After 1 h, the reactions were stopped with NaOH (500 mM) and plates were read at 405 nm. Concentrated medium alone or 10 pg/ml purified mouse EGF, HB-EGF, and TGF-α were used as negative and positive controls, respectively.

Detection of ROS. ROS production was measured with dihydrorhodamine as previously described (4). Briefly, 15×10^4 mesangial cells were plated in six-well plates in Dulbecco modified Eagle medium (DMEM) containing 1% fetal calf serum (FCS) with or without AG1478 (300 nM). After 2 days, 2 μM dihydrorhodamine (Sigma) was added to the wells. After 2 h, cells were trypsinized and generation of fluorescent rhodamine 123 was analyzed by a FACScan. Three independent experiments were performed in triplicate.

Adhesion assay. A cell adhesion assay was performed as previously described (4). Briefly, 96-well plates were coated with fibronectin or collagen IV (both at 10 μg/ml) for 1 h at 37°C. After blocking of nonspecific adhesion with 1% BSA in PBS, 5×10^4 mesangial cells in 100 μl serum-free DMEM were added to the

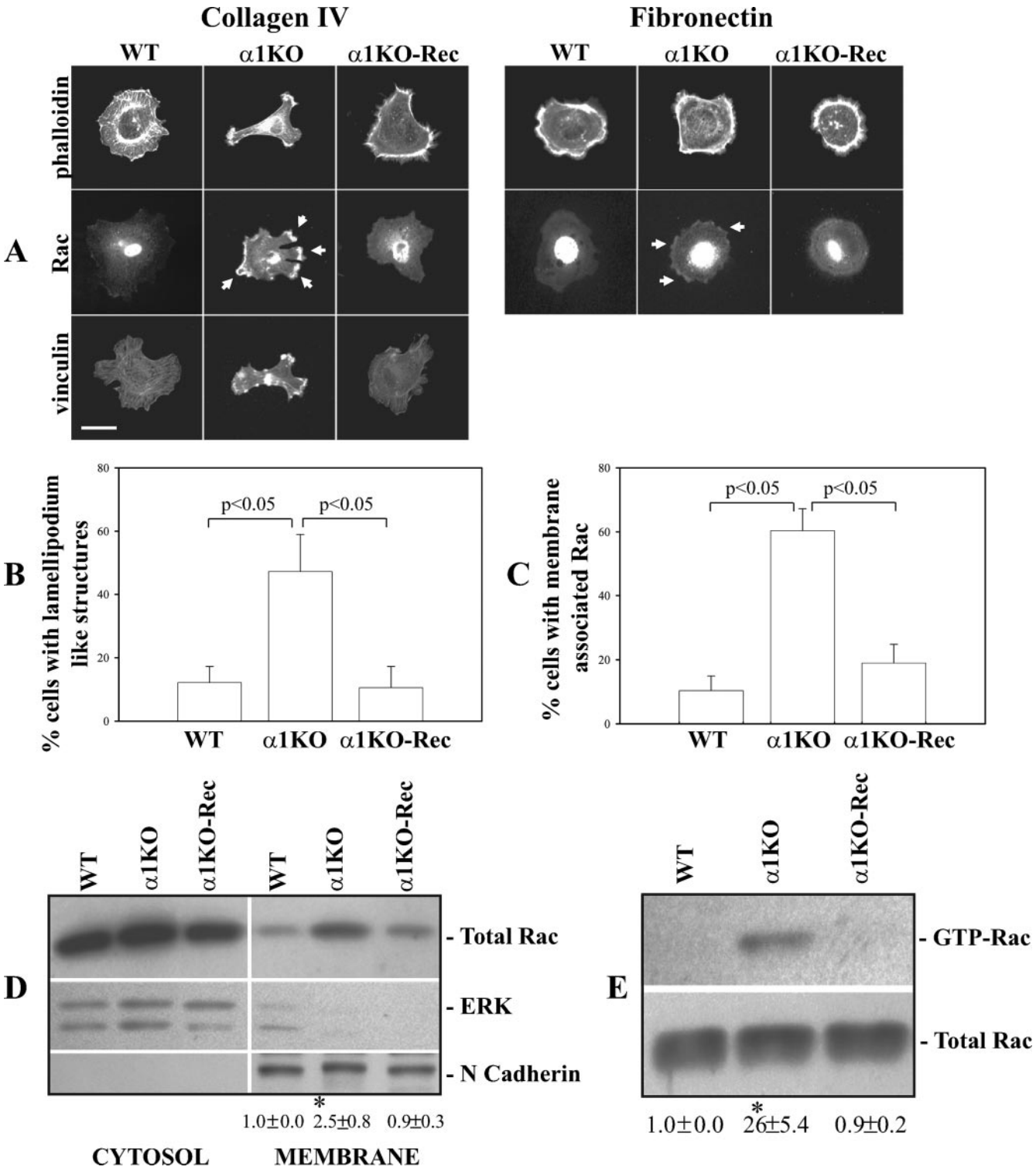

FIG. 2. Increased membrane-bound and activated Rac1 in integrin α1KO mesangial cells. (A) Mesangial cells were serum starved for 24 h and plated for 3 h on collagen IV or fibronectin (10 μg/ml each), after which they were stained with rhodamine-phalloidin, anti-Rac1, or anti-vinculin antibodies. The arrows indicate membrane-bound Rac1. Scale bar, 10 μm. (B, C) The percentage of cells plated on collagen IV that exhibited lamellipodium-like structures (B), as well as membrane-associated Rac (C), was quantified. Values are the mean ± standard deviation of three experiments (n = 200 cells). (D) Mesangial cells were plated on uncoated dishes, incubated for 48 h, and subsequently serum starved for 24 h. Equal amounts of cytosol and membrane fractions (40 μg/lane) were then analyzed by Western blotting with anti-Rac antibodies. Membranes were then incubated with anti-ERK or anti-N-cadherin antibodies to verify equal loading and purity of the preparation. Rac and N-cadherin bands in membrane fractions were quantified by densitometry analysis, and the Rac signal is expressed as the Rac/N-cadherin ratio. Values are the mean ± standard deviation of three experiments and represent changes (n-fold) relative to WT cells. The asterisk is as in Fig. 1D. (E) Eight hundred micrograms of total cell lysate of mesangial cells incubated as described for panel D was incubated with glutathione *S*-transferase–PBD beads. Bound GTP-Rac was detected by Western blotting with anti-Rac1 antibody (top). Forty micrograms of total cell lysate was used to detect the levels of total Rac1 (bottom). GTP-Rac and Rac bands were quantified by densitometry analysis, and the activated Rac signal is expressed as the GTP-Rac/N-cadherin ratio. Values and asterisks are as described for panel D.

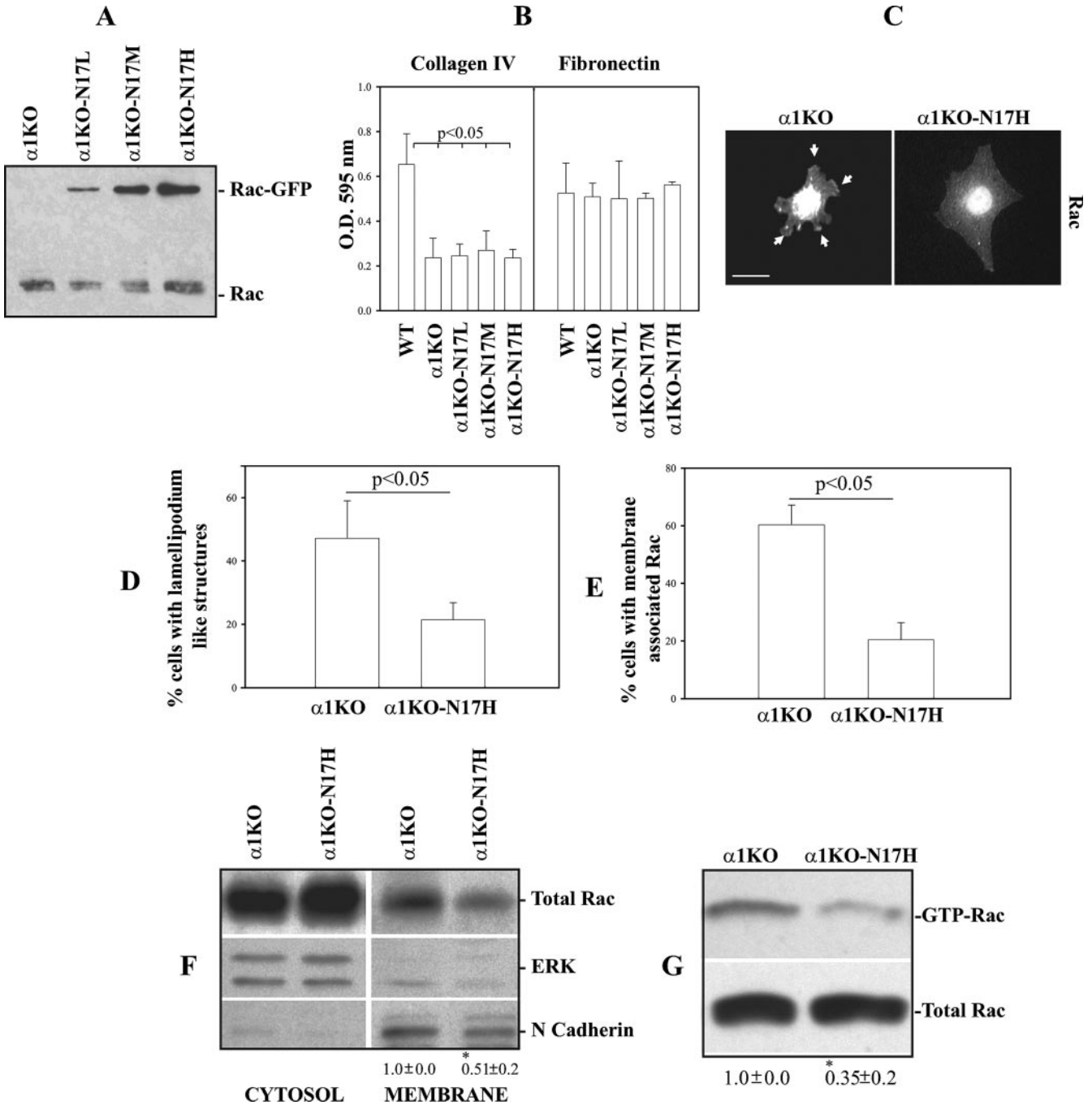

FIG. 3. Dominant negative Rac1 decreases membrane-bound and activated Rac1 in integrin α1KO mesangial cells. (A) α1KO mesangial cells were transfected with either GFP vector (α1KO) or dominant negative GFP-N17Rac (α1KO-N17) and sorted by FACS into three different cell populations on the basis of levels of GFP (low, medium, high). Endogenous Rac1 and GFP-N17Rac were detected by Western blotting with anti-Rac1 antibody (40 μg cell lysate/lane). (B) Mesangial-cell adhesion on collagen IV or fibronectin (10 μg/ml each) was determined as described in Materials and Methods. Values represent the mean ± standard deviation of three experiments performed in quadruplicate. (C) Serum-starved mesangial cells were plated on collagen IV (10 μg/ml) and incubated for 3 h, and Rac localization was analyzed with anti-Rac antibodies. Arrows represent membrane-associated Rac. Scale bar, 10 μm. (D, E) The percentages of cells plated on collagen IV that exhibited lamellipodium-like structures (D) and membrane-associated Rac (E) were quantified. Values are the mean ± standard deviation of three experiments ($n = 150$ cells). (F) Cytosol and membrane fractions (40 μg/lane) of mesangial cells were analyzed by Western blotting with anti-Rac antibodies. Membranes were subsequently incubated with anti-ERK or anti-N-cadherin antibodies to verify equal loading and the purity of the preparation. Rac and N-cadherin bands in membrane fractions were quantified and expressed as described in the legend to Fig. 2D. Values are the mean ± standard deviation of three experiments and represent changes (n-fold) relative to α1KO cells. An asterisk indicates a significant difference ($P < 0.05$) between α1KO and α1KO-N17H cells. (G) Eight hundred micrograms of total mesangial-cell lysate was incubated with glutathione S-transferase–PBD beads, and bound GTP-Rac or total Rac was detected by Western blotting. GTP-Rac and Rac bands were quantified and expressed as described in the legend to Fig. 2E. Values and asterisks are as already described.

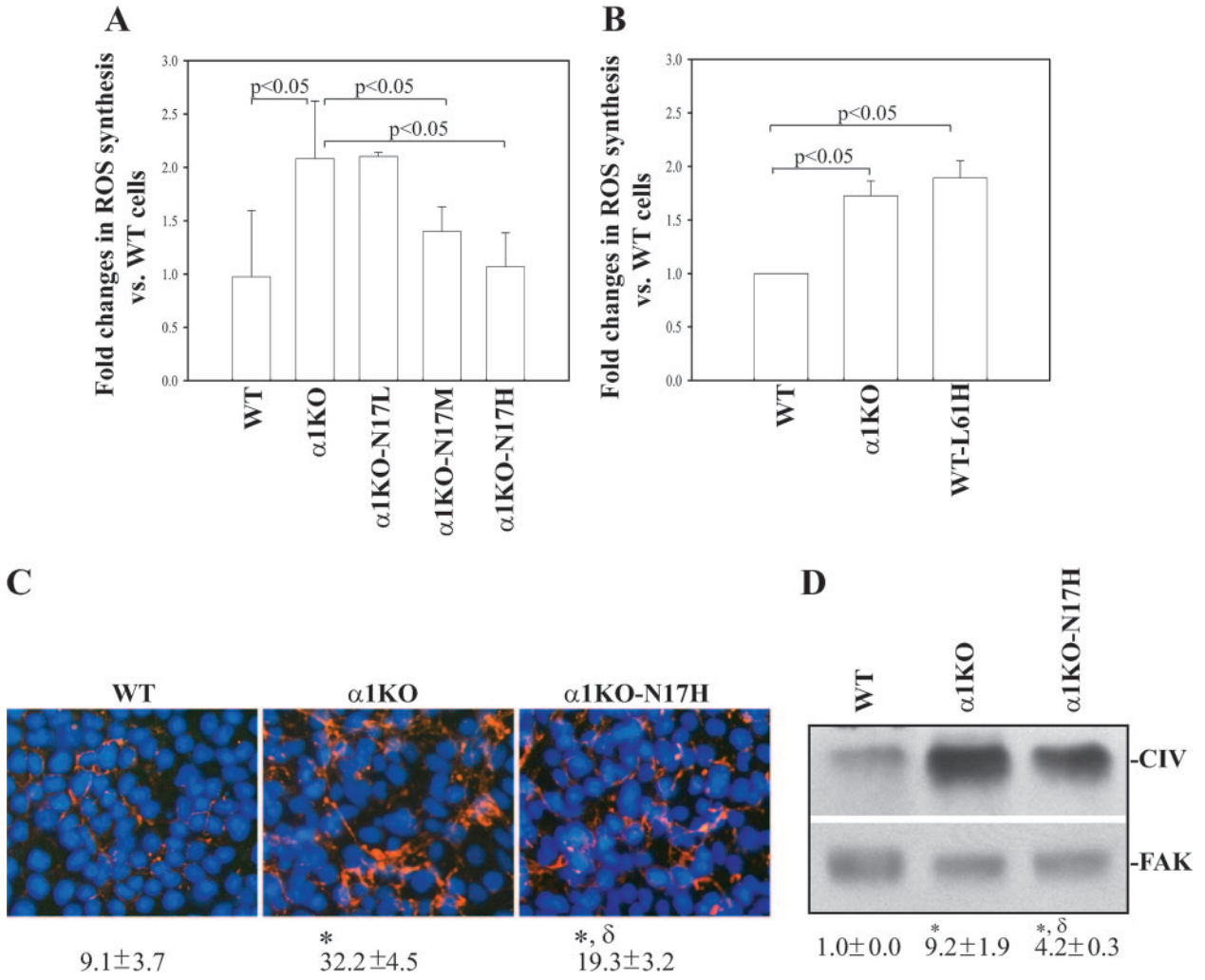

FIG. 4. Dominant negative Rac1 partially decreases ROS generation and collagen deposition in integrin α1KO mesangial cells. (A, B) Mesangial cells (15×10^4/well) were plated on uncoated six-well plates in DMEM containing 1% FCS. After 2 days, 2 μM dihydrorhodamine was added and ROS generation was evaluated as described in Materials and Methods. Values represent the mean ± standard deviation of three experiments performed in triplicate. (C) Mesangial cells were cultured as described in the legend to Fig. 1D, and collagen IV deposition was evaluated by indirect immunofluorescence assay. The percentage of the area occupied by collagen IV-positive structures per microscopic field was quantified with the Scion Image program as described in Materials and Methods. Values are the mean ± standard deviation of four experiments. Differences between WT and α1KO cells (∗) or α1WT and α1KO-N17H cells (δ) were significant at $P < 0.05$. (D) Collagen IV (CIV) levels in cell lysates (40 μg/lane) were detected by Western blot analysis and are expressed as described in the legend to Fig. 1E. Symbols (∗ and δ) are as already described.

plates and incubated for 1 h at 37°C. After removal of nonadherent cells, the cells were fixed with 4% formaldehyde, stained with 1% crystal violet, solubilized in 20% acetic acid, and then read at 595 nm. Cell adhesion to 1% BSA-coated wells was subtracted from the values obtained with extracellular-matrix proteins. Three independent experiments were performed in quadruplicate.

Statistical analysis. The Student *t* test was used for comparisons between two groups, and analysis of variance with Sigma-Stat software was used for determination of statistically significant differences among multiple groups. $P < 0.05$ was considered statistically significant.

RESULTS

Increased ROS and collagen synthesis by α1-null mesangial cells is a direct consequence of the loss of this collagen binding receptor. We previously reported that integrin α1-null (α1KO) mesangial cells have upregulated collagen synthesis relative to their WT counterparts at both RNA and protein levels (4, 14). This is both due to an increase in ROS production and a direct consequence of the loss of the negative regulatory effect of the α1β1 integrin (4). To determine whether these observations in integrin α1KO mesangial cells were a direct consequence of loss of α1β1, we generated populations of integrin α1KO mesangial cells expressing the human integrin α1 subunit (α1KO-Rec) (Fig. 1A). To ensure functionality of the human subunit, WT, α1KO (transfected with vector only), and α1KO-Rec cells were plated on either collagen IV (a major integrin α1β1 binding ligand) or fibronectin (an integrin α1β1-independent ligand) and their adhesion was evaluated 1 h after plating. As previously described (15), α1KO cells showed an ~60% reduction in adhesion on collagen IV compared to their WT counterparts (Fig. 1B), while α1KO-Rec cells were able to adhere to collagen IV as well as WT cells (Fig. 1B). No differences in

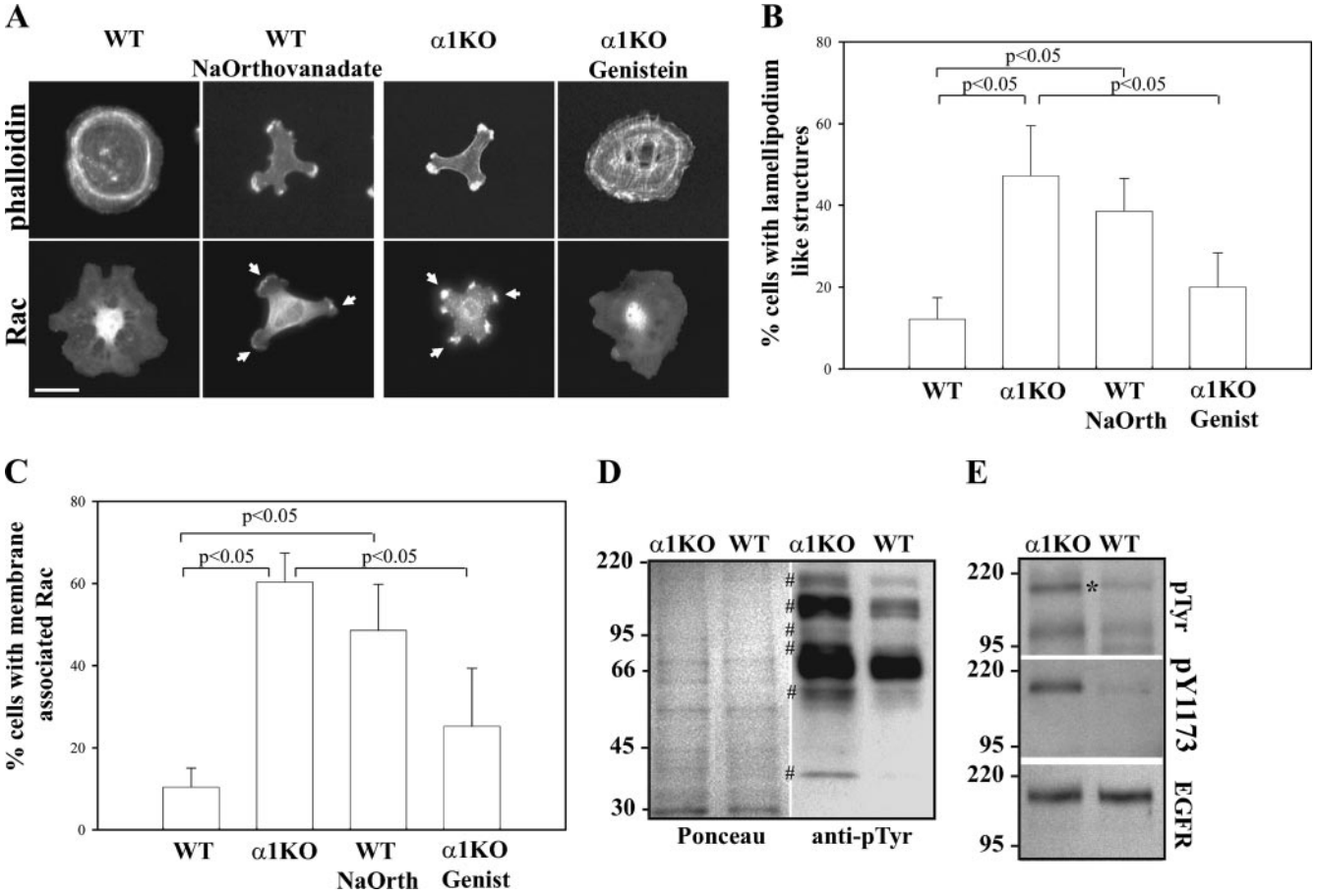

FIG. 5. Increased tyrosine phosphorylation in integrin α1KO mesangial cells leads to increased membrane-bound Rac1. (A) Mesangial cells were serum starved for 24 h with or without Na orthovanadate (25 μM) or genistein (20 μM). Cells were subsequently plated for 3 h on collagen IV (10 μg/ml) with or without Na orthovanadate (5 μM) or genistein (5 μM) and stained with rhodamine-phalloidin or anti-Rac1 antibodies. The arrowheads indicate membrane-bound Rac1. Scale bar, 10 μm. (B, C) The percentages of cells plated on collagen IV that exhibited lamellipodium-like structures (B) and membrane-associated Rac (C) were quantified. Values are the mean ± standard deviation of three experiments ($n = 150$ cells). (D) Total tyrosine phosphorylation in serum-starved cells was determined with an anti-phosphotyrosine antibody (40 μg total cell lysate/lane). The symbol # indicates tyrosine-phosphorylated proteins highly increased in α1KO cells. (E) Mesangial-cell lysates (40 μg/lane) prepared as described for panel D were analyzed by Western blotting with antiphosphotyrosine, anti-pY1173, and anti-EGFR antibodies. The asterisk indicates the position of the EGFR. The values on the left are molecular sizes in kilodaltons.

adhesion on fibronectin were observed among the three different cell types (Fig. 1B). α1KO-Rec cells also produced ROS (Fig. 1C) and collagen (Fig. 1D and E) to levels observed in WT cells. These findings demonstrate that the increased ROS and collagen deposition in the α1KO cells is a direct consequence of the loss of this receptor. In addition, it verifies that the properties of the WT and α1KO-Rec cells are the same with respect to integrin α1β1-dependent functions.

Integrin α1KO mesangial cells show increased basal levels of activated Rac1. To define the mechanism underlying the increased basal ROS production in integrin α1KO mesangial cells, we investigated the activation state and localization of Rac1. This small GTPase can serve as an adapter to position $p67^{phox}$ for interaction with the membrane-bound cytochrome b_{558} (reviewed in reference 2). Moreover, Rac and consequent ROS synthesis can be transiently activated by integrin clustering in various cell types, including fibroblasts and platelets (11, 27, 49, 54).

Despite their weak cell-adhesive properties on collagen substrata, α1KO mesangial cells that adhere to collagen IV (~40% compared to WT cells; Fig. 1B) showed an altered morphology compared to their WT counterparts. While WT cells spread and expressed an extensive network of actin filaments and stress fibers (Fig. 2A and B), α1KO cells did not spread and developed multiple lamellipodia, membrane ruffles, and subcortical F-actin at the leading edge of the cells (Fig. 2A and B), similar to cells overexpressing constitutively active Rac1 (13, 46). Reexpression of the integrin α1 subunit in α1KO cells reverted the phenotype to that observed in WT cells (Fig. 2A and B). The peculiar phenotype of the α1KO cells was only visible on collagen IV, as all three cell types spread equally and showed similar networks of actin filaments and stress fibers when plated on fibronectin (Fig. 2A). Immunofluorescence assay revealed increased amounts of membrane-associated Rac1 in integrin α1KO cells plated on collagen IV compared to WT or α1KO-Rec cells (Fig. 2A and C). Moreover, membrane-bound Rac1 localized to areas that contained vinculin (Fig. 2A) and phosphopaxillin (not shown), two proteins found in abundance in focal complexes (56). Although

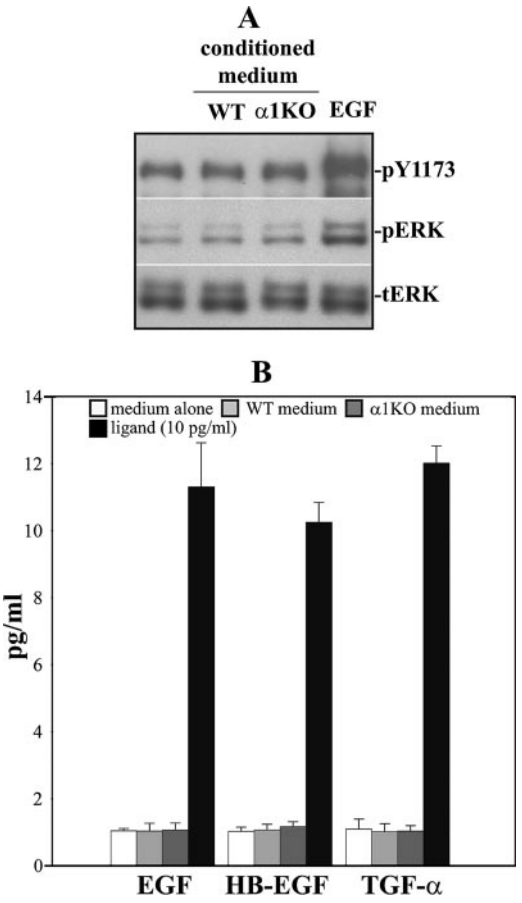

FIG. 6. WT and α1KO mesangial cells do not secrete detectable levels of EGFR ligands. (A) Serum-starved A431 cells were kept untreated, treated with medium conditioned for 72 h with WT and α1KO mesangial cells, or treated with 10 ng/ml EGF. After 10 min, total cell lysates (5 μg/lane) were analyzed by Western blotting for phosphorylated EGFR, as well as phosphorylated and total ERK. (B) One hundred microliters of medium conditioned for 72 h with WT and α1KO mesangial cells was used to analyze the levels of secreted EGF, HB-EGF, and TGF-α by ELISA (see Materials and Methods for details). Concentrated medium alone or 10 pg/ml purified mouse EGF, HB-EGF, or TGF-α was used as a negative or positive control, respectively.

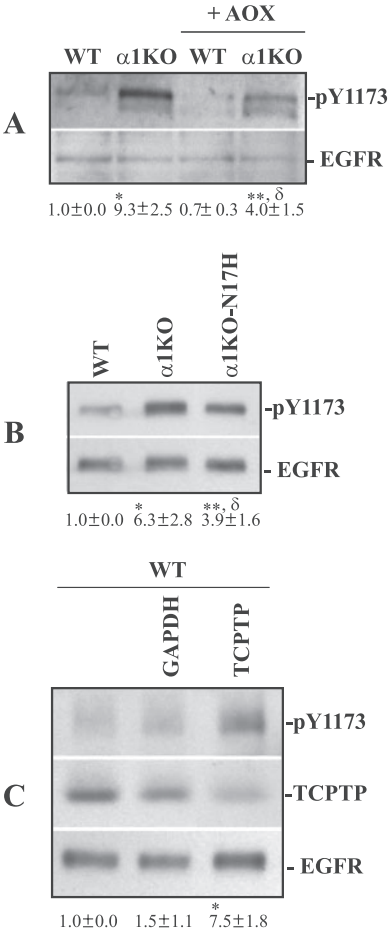

FIG. 7. ROS partially contribute to increased EGFR phosphorylation in integrin α1KO mesangial cells. (A) Mesangial cells were serum starved for 24 h with or without antioxidants (AOX) (see Materials and Methods for details), and total cell lysates (40 μg/lane) were analyzed by Western blotting with anti-pY1173 or anti-EGFR antibodies. Phosphorylated and total EGFR bands were quantified by densitometry analysis, and phosphorylated EGFR is expressed as the pY1173/EGFR ratio. Values are the mean ± standard deviation of three experiments and are expressed as changes (*n*-fold) relative to WT cells. Differences between WT and α1KO (∗), WT and α1KO+AOXs (∗∗), or α1KO and α1KO+AOXs (δ) cells were significant at $P < 0.05$. (B) The mesangial cells indicated were serum starved for 24 h, and the levels of phosphorylated and total EGFR were analyzed by Western blotting. Phosphorylated EGFR bands were quantified and expressed as indicated above. Differences between WT and α1KO (∗), WT and α1KO-N17H (∗∗), or α1KO and α1KO-N17H (δ) cells were significant at $P < 0.05$. (C) Cell lysates (40 μg/lane) of serum-starved WT mesangial cells either left untransfected or transfected with the siRNAs indicated were analyzed by Western blotting with anti-pY1173, anti-TCPTP, and anti-EGFR antibodies. Phosphorylated EGFR and TCPTP bands were quantified by densitometric analysis and normalized to total EGFR bands. Values are the mean ± standard deviation of three experiments and are expressed as changes (*n*-fold) in pY1173/TCPTP relative to WT cells. Differences between untransfected and TCPTP siRNA-transfected cells (∗) were significant at $P < 0.05$. GAPDH, glyceraldehyde-3-phosphate dehydrogenase.

less evident, membrane-associated Rac1 was also seen in the α1KO cells plated onto fibronectin (Fig. 2A). Increased membrane-associated Rac1 in α1KO cells was also confirmed by Western blot analysis of membrane-enriched fractions (Fig. 2D).

Since it has been shown that activated Rac1 (i.e., GTP-Rac) is recruited to the plasma membrane (10), we analyzed the levels of GTP-Rac and found that α1KO cells also have elevated basal levels of activated Rac compared to WT cells (Fig. 2E). As expected, reexpression of the integrin α1 subunit in α1KO cells significantly decreased levels of both membrane-bound and GTP-bound Rac1 (Fig. 2A, C, D, and E). Thus, loss of integrin α1β1 leads to increased levels of activated and membrane-bound Rac1, which is independent of the ligand on which the cells are plated.

Dominant negative Rac decreases both membrane-bound Rac and ROS synthesis in α1KO mesangial cells. To determine the contribution of activated Rac to both ROS and collagen synthesis, α1KO mesangial cells were transfected with GFP-labeled dominant negative Rac1 (GFP-N17Rac) and sorted by fluorescence-activated cell sorter (FACS) into low-, medium-, and high-expressing cell populations on the basis of the levels of GFP (α1KO-N17L, α1KO-N17M, and α1KO-

N17H) (Fig. 3A). Dominant negative Rac1 did not alter the ability of α1KO cells to adhere to collagen IV, as α1KO-N17 cells adhere to collagen IV as well as vector-transfected α1KO cells (Fig. 3B). In addition, all three cell populations showed similar adhesion to fibronectin (Fig. 3B), suggesting that N17Rac did not alter integrin expression and/or avidity for ligand. Despite similar adhesion, α1KO-N17 cells (only cell populations expressing high levels of N17Rac are shown) spread more on collagen IV and show less lamellipodium-like structures (Fig. 3C and D) compared to vector-transfected α1KO mesangial cells (Fig. 3C and D). Moreover, α1KO-N17 cells showed decreased membrane-bound (Fig. 3C, E, and F), as well as GTP-bound, Rac1 (Fig. 3G) compared to vector-transfected α1KO mesangial cells. These findings confirm that activation of Rac1 is sufficient to mediate cytoskeletal reorganization (52) and downregulation of endogenous Rac1 is sufficient to reduce peripheral lamellipodia and promote cell spreading (42).

α1KO-N17 cells also showed reduced ROS synthesis, and the maximum reduction was observed in α1KO-N17H cells which produced ROS at levels of vector-transfected WT cells (Fig. 4A). To further confirm the role of Rac in the control of ROS production, WT mesangial cells were transfected with GFP-labeled, activated Rac1 (GFP-L61Rac) and ROS synthesis was compared to that of WT and α1KO cells transfected with the vector only. WT-L61 cells expressing high levels of GFP produced ROS at levels of α1KO cells (Fig. 4B), confirming a positive role for Rac1 in ROS generation. Interestingly, although α1KO-N17H cells produced ROS levels similar to those of WT cells (Fig. 4A), they only partially reduced collagen IV deposition compared to WT (Fig. 4C and D) or α1KO-Rec (Fig. 1D and E) cells, suggesting that an integrin α1-dependent, ROS-independent mechanism is also involved in the control of collagen synthesis.

Integrin α1KO mesangial cells show increased basal levels of activated EGFR. Activation of Rac1 can be mediated by multiple mechanisms, including activation of tyrosine kinase receptors, such as the EGFR (38, 51). It has been shown that loss of integrin α1β1 leads to upregulated EGFR tyrosine phosphorylation (39). In addition, ROS can initiate a number of physiological responses, including tyrosine phosphorylation of growth factor receptors, such as platelet-derived growth factor receptor and EGFR (23). For this reason, we determined whether increased levels of tyrosine phosphorylation might account for the increase in Rac1 activation in α1KO mesangial cells. To test this hypothesis, we treated WT cells with the tyrosine phosphatase inhibitor Na orthovanadate and the α1KO cells with the tyrosine kinase inhibitor genistein. Na orthovanadate-treated WT cells plated on collagen IV not only acquired a morphology that resembled that of α1KO cells (Fig. 5A and B) but also showed increased membrane-associated Rac1 (Fig. 5A and C). In contrast, genistein-treated α1KO cells acquired a phenotype similar to that of WT cells, spread normally, and lost membrane-associated Rac1 (Fig. 5A to C). We therefore assessed whether there were differences in tyrosine phosphorylation levels between α1KO and WT mesangial cells by performing Western blot analysis on serum-starved cell lysates with an anti-phosphotyrosine antibody. As shown in Fig. 5D, increased basal levels of tyrosine-phosphorylated proteins were detected in the lysates of α1KO mesangial cells, with at least six bands (~170 kDa, ~110 kDa, ~95 kDa, ~70 kDa, ~50 kDa, and ~40 kDa) more prominent. Treatment of WT cells with Na orthovanadate significantly increased, while treatment of α1KO cells with genistein significantly decreased, the levels of these bands (data not shown), suggesting a correlation among levels of tyrosine-phosphorylated proteins, cell morphology, and Rac localization. As the EGFR runs at a molecular mass of ~170 kDa and it is known that both integrin α1β1 (39) and ROS (23) can modulate its activation status, we determined whether the highly phosphorylated band observed at ~170 kDa was the EGFR. Lysates of serum-starved WT and α1KO mesangial cells, analyzed by Western blotting with a specific phospho-EGFR antibody, revealed increased basal levels of phosphorylated EGFR in α1KO mesangial cells (Fig. 5E).

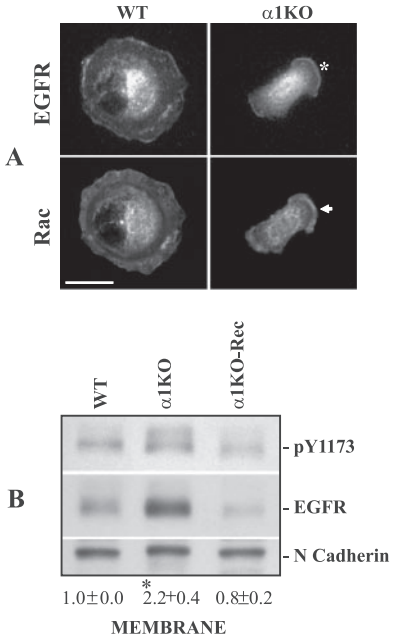

FIG. 8. Increased membrane-associated EGFR in integrin α1KO mesangial cells. (A) Mesangial cells were serum starved for 24 h, subsequently plated for 3 h on collagen IV (10 μg/ml), and double stained with anti-EGFR and anti-Rac1 antibodies. The asterisk and arrow indicate localization of membrane-associated EGFR and Rac, respectively. Scale bar, 10 μm. (B) Membrane fractions (40 μg/lane) from mesangial cells were analyzed by Western blotting with anti-pY1173 and anti-EGFR antibodies. Membranes were subsequently incubated with anti-N-cadherin antibodies to verify equal loading. pY1173 and N-cadherin bands were quantified by densitometric analysis, and the results are expressed as the pY1173/N-cadherin ratio. Values are the mean ± standard deviation of three experiments and represent changes (*n*-fold) relative to WT cells. Differences between WT and α1KO cells (*) were significant at $P < 0.05$.

Increased basal levels of activated EGFR in α1KO mesangial cells are ligand independent. We next investigated whether increased levels of phosphorylated EGFR in the α1KO mesangial cells were due to excessive EGF secretion. To do this, we exposed A431 cells, known to express high levels of EGFR (29), to medium conditioned for 72 h with WT and integrin α1KO mesangial cells, following which the activity of their EGFR was analyzed. As shown in Fig. 6A, no activation of EGFR or downstream ERK was observed in A431 cells incubated with medium conditioned with either WT or integrin α1KO cells, unlike cells treated with 10 ng/ml recombinant

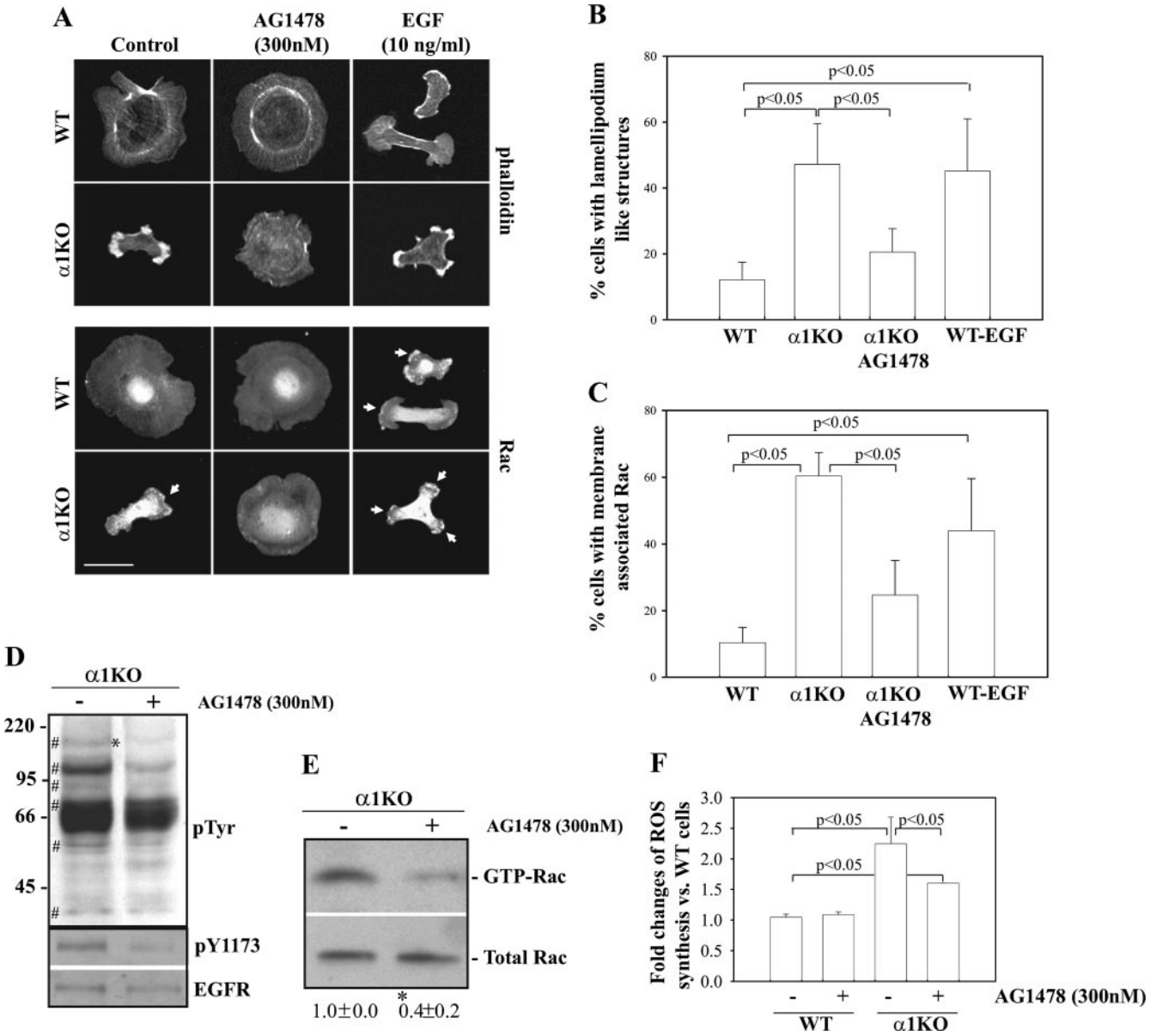

FIG. 9. Increased EGFR phosphorylation in integrin α1KO mesangial cells upregulates Rac1 activation and ROS generation. (A) Mesangial cells serum starved for 24 h with or without AG1478 (300 nM) were plated onto collagen IV (10 μg/ml), incubated for 3 h with or without AG1478 (300 nM) or EGF (100 ng/ml), and stained with rhodamine-phalloidin or anti-Rac1 antibody. The arrows indicate membrane-bound Rac1. Scale bar, 10 μm. (B, C) The percentages of cells plated on collagen IV that exhibited lamellipodium-like structures (B) and membrane-associated Rac (C) were quantified. Values are the mean ± standard deviation of three experiments (n = 150 cells). (D) α1KO cells were serum starved for 24 h as indicated for panel A, and cell lysates (40 μg/lane) were analyzed by Western blotting with anti-phosphotyrosine, anti-pY1173, and anti-EGFR antibodies. The symbol # indicates tyrosine-phosphorylated proteins highly increased in α1KO cells, while the asterisk indicates the position of the EGFR. The values on the left are molecular sizes in kilodaltons. (E) α1KO cells were serum starved for 24 h as indicated for panel A, and GTP-Rac or total Rac1 levels were detected as described in the legend to Fig. 2C. GTP-Rac and Rac bands were quantified and expressed as described in the legend to Fig. 2E. Values are the mean ± standard deviation of three experiments and represent changes (n-fold) relative to untreated α1KO cells. The asterisk indicates a significant difference ($P < 0.05$) between untreated and AG1478-treated cells. (F) Mesangial cells were plated in six-well plates at a density of 15×10^4/well in DMEM containing 1% FCS with or without AG1478 (300 nM). After 2 days, 2 μM dihydrorhodamine was added to the wells and ROS generation was evaluated. Values represent the mean ± standard deviation of three independent experiments performed in triplicate.

EGF. Similarly, no measurable levels of secreted EGFR ligands (i.e., EGF, HB-EGF, and TGF-α) were detected by ELISA (Fig. 6B), thus confirming that activation of the EGFR in the α1KO cells is indeed a ligand-independent event.

ROS-dependent and -independent mechanisms are responsible for EGFR activation in α1KO mesangial cells. As ROS can induce EGFR activation (23), we treated mesangial cells with the antioxidants TEMPOL and diphenyleneiodium (see

Materials and Methods for details). Although the phosphorylation levels of EGFR markedly decreased in antioxidant-treated WT and integrin α1KO cells (Fig. 7A), more phosphorylated receptor was still evident in the antioxidant-treated α1KO cells (Fig. 7A). To further confirm our finding, we compared the levels of phosphorylated EGFR in WT, α1KO, and α1KO-N17H cells. Although α1KO-N17H and WT cells produce similar levels of ROS (Fig. 4A), α1KO-N17H showed more activated EGFR than WT cells (Fig. 7B); however, this activation was less than in α1KO cells. This result suggests that both ROS-dependent and ROS-independent mechanisms are responsible for EGFR activation in α1KO cells. Since integrin α1β1 negatively regulates EGFR activation by recruiting or activating the protein tyrosine phosphatase TCPTP (39), we determined the contribution of this phosphatase in EGFR activation in mesangial cells. WT mesangial cells were therefore depleted of endogenous TCPTP by siRNA, and the levels of phosphorylated EGFR were compared to those of WT cells transfected with a control siRNA. As shown in Fig. 7C, down-regulation of TCPTP resulted in increased basal levels of EGFR phosphorylation, demonstrating that this phosphatase negatively regulates EGFR activation in mesangial cells.

EGFR activation is required for the altered cell morphology and activation of Rac1 in α1KO mesangial cells. We next analyzed the localization of EGFR in mesangial cells plated on collagen IV. Uniform distribution of the receptor was detected on the WT cell surface, while in α1KO cells abundant levels of membrane-associated EGFR were found to cluster in lamellipodium-like structures like membrane-bound Rac1 (Fig. 8A). Membrane fractions, prepared from serum-starved mesangial cells, confirmed that α1KO cells have more membrane-bound, as well phosphorylated, EGFR compared to WT or α1KO-Rec cells (Fig. 8B), thus paralleling the distribution of Rac (Fig. 2D).

To determine whether EGFR was responsible for the altered cell morphology and activation of Rac1 in α1KO mesangial cells, mesangial cells were treated with AG1478, a specific EGFR inhibitor that inhibits the kinase activity of the receptor in a ligand-independent fashion. Integrin α1KO mesangial cells treated with AG1478 acquired a morphology that resembled that of WT cells and lost membrane-associated Rac1 (Fig. 9A to C). In contrast, WT cells treated with EGF ligand acquired a phenotype similar to that of α1KO mesangial cells and became elongated and developed lamellipodia, membrane ruffling, and membrane-associated Rac1 (Fig. 9A to C), typical of cells treated with EGF ligand (31). To confirm that the phenotype observed in AG1478-treated α1KO cells was due to attenuation of EGFR signaling, we initially analyzed tyrosine phosphorylation levels in α1KO cells left untreated or treated with AG1478. As expected, the phosphorylation levels of the protein at ~170 kDa decreased in the AG1478-treated α1KO cells (Fig. 9D). Interestingly, the phosphorylation levels of two other bands (~110 kDa and ~95 kDa) also significantly decreased in the AG1478-treated α1KO cells (Fig. 9D), suggesting that these proteins are EGFR substrates. Finally, treatment with AG1478 led to decreased levels of phosphorylated EGFR (Fig. 9D), reduced membrane-associated (Fig. 9A and C) and GTP-bound Rac1 (Fig. 9E), and decreased ROS synthesis (Fig. 9F). Thus, increased levels of activated EGFR in α1KO cells lead to increased levels of activated membrane-associated Rac1 and consequent ROS generation.

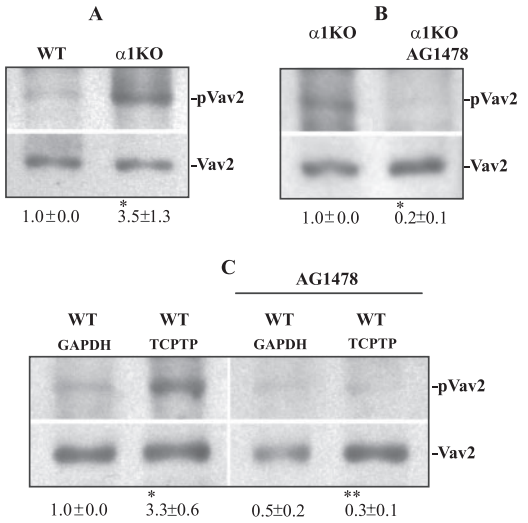

FIG. 10. Increased basal levels of phosphorylated Vav2 in α1KO mesangial cells. (A) Mesangial cells were plated on uncoated dishes, incubated for 48 h, and subsequently serum starved for 24 h. Forty micrograms of cell lysate was then analyzed by Western blotting with anti-pVav2 (Tyr-172) or anti-Vav2 antibodies. pVav2 and Vav2 bands were quantified by densitometry analysis, and the pVav2 signal is expressed as the pVav2/Vav2 ratio. Values are the mean ± standard deviation of three experiments and represent changes (*n*-fold) relative to WT cells. Differences between WT and α1KO cells (∗) were significant at $P < 0.05$. (B) α1KO mesangial cells incubated as described above were serum starved for 24 h with or without AG1478 (300 nM). Forty micrograms of cell lysate was analyzed by Western blotting with the antibodies indicated above. pVav2 and Vav2 bands were quantified, and the results are expressed as indicated above. Values are the mean ± standard deviation of three experiments and represent changes (*n*-fold) relative to untreated α1KO cells. Differences between untreated and AG1478-treated cells (∗) were significant at $P < 0.05$. (C) WT mesangial cells transfected with the siRNAs indicated were serum starved for 24 h with or without AG1478 (300 nM). Forty micrograms of cell lysate was analyzed by Western blotting with the antibodies indicated above. pVav2 and Vav2 bands were quantified and expressed as indicated above. Values are the mean ± standard deviation of three experiments and are expressed as changes (*n*-fold) relative to untreated WT cells transfected with GAPDH (glyceraldehyde-3-phosphate dehydrogenase) siRNA. Differences between GAPDH siRNA versus TCPTP siRNA-transfected cells (∗) and TCPTP siRNA versus TCPTP siRNA-plus-antioxidant cells (∗∗) were significant at $P < 0.05$.

Vav2 is involved in EGFR-mediated Rac activation in α1KO mesangial cells. We finally investigated whether the GEF Vav2 might be involved in increased Rac activation in α1KO cells. We focused on Vav2, as (i) this GEF, unlike Vav1 and Vav3, is ubiquitously expressed; (ii) mesangial cells express this Vav family member (Fig. 10A); (iii) EGFR controls Rac activation via Vav2 tyrosine phosphorylation (51); (iv) we observed a prominent tyrosine-phosphorylated band at ~110 kDa in α1KO cells (Fig. 5D), and (v) phosphorylation of this ~110-kDa band was significantly decreased following AG1478 treatment (Fig. 9D).

Interestingly, increased basal levels of phosphorylated Vav2 (Tyr-172) were observed in α1KO mesangial cells compared to those in WT cells (Fig. 10A). Treatment of α1KO cells with AG1478 significantly decreased the levels of activated Vav2 (Fig. 10B), confirming that EGFR positively controls Vav2 activation in mesangial cells.

As integrin-activated protein tyrosine phosphatases can di-

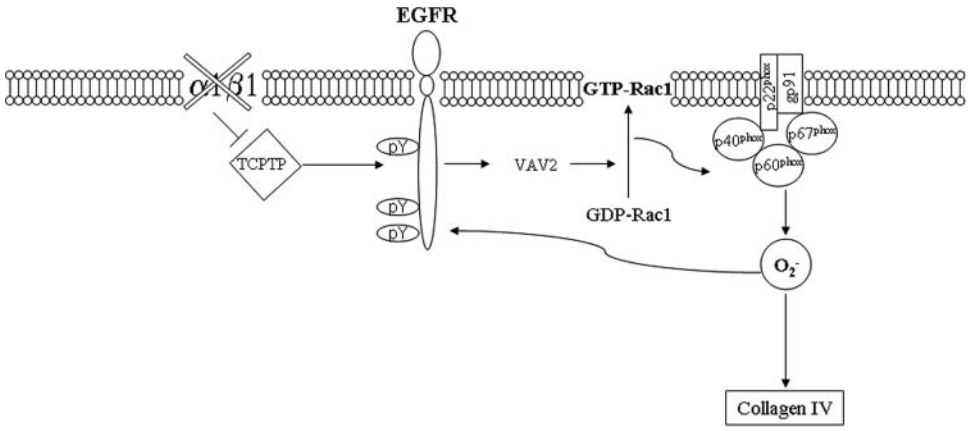

FIG. 11. Regulation of ROS and collagen synthesis in α1KO mesangial cells. Schematic model of how ROS (O_2^-) and collagen might be regulated in α1KO mesangial cells. Lack of integrin α1β1 results in increased EGFR phosphorylation, Vav2 recruitment, Rac1 activation, and NAPDH-mediated O_2^- production. Increased O_2^- can subsequently lead to both enhanced collagen IV synthesis and EGFR phosphorylation.

rectly downregulate Vav1 activation in neutrophils (59), the levels of phosphorylated Vav2 were analyzed in WT cells transfected with TCPTP siRNA. As shown in Fig. 10C, downregulation of TCPTP resulted in increased basal levels of activated Vav2. However, this activation was completely inhibited in TCPTP siRNA-transfected WT cells incubated in the presence of AG1478 (Fig. 10C). Together, these data strongly indicate that EGFR is the major, if not the only, activator of Vav2 in mesangial cells, as inhibition of TCPTP expression increased Vav2 phosphorylation by enhancing EGFR phosphorylation.

DISCUSSION

Mice lacking integrin α1β1 develop increased glomerular sclerosis following renal injury, which is characterized by increased collagen IV production by mesangial cells in part because of excessive ROS production (4). In the present study, we provide evidence that excessive ROS and collagen IV production by α1KO mesangial cells is due to increased Rac1 activation mediated by constitutive EGFR phosphorylation. These results define a novel mechanism whereby integrin α1β1 regulates the production of ROS and collagen, both of which are critical components in the development of fibrosis, the final common pathway of end organ damage in multiple diseases.

α1KO mesangial cells plated on collagen IV have a striking phenotype characterized by multiple lamellipodia, membrane ruffles, and subcortical F-actin at the leading edge of the cells. This phenotype is consistent with the observations that activation of Rac induces formation of lamellipodia (41) and resembles that of cells overexpressing constitutively active Rac1 (13, 46). The requirement of Rac activation for this alteration in cell morphology was confirmed by reversal of the phenotype following transfection with dominant negative N17Rac. Phenotypical changes and spreading of α1KON17 cells were directly proportional to the amount of dominant negative Rac, and this is consistent with the finding that a 30 to 50% reduction in endogenous Rac1 is sufficient to reduce the number of peripheral lamellipodia (42). Despite high expression of N17Rac, α1KO mesangial cells did not spread as much as WT cells on collagen, implying that both Rac and loss of integrin α1β1 contribute to cell shape on collagen substrata. Interestingly, the lamellipodium-like structures are not observed when α1KO cells are plated on fibronectin, although these cells still show membrane-bound Rac. The reason for this is unclear; however, it is conceivable that cell spreading promoted by non-collagen binding receptors (i.e., α5β1 or αvβ1) might be sufficient to compensate for the Rac-induced lamellipodium formation.

In addition to the alterations in cell morphology, we provide the novel observation that upregulated Rac1 activation in α1KO mesangial cells results in a ROS-dependent increase in collagen IV synthesis. As Rac GTPase is required for NADPH oxidase activity (reviewed in reference 2), the increased activation of Rac1 in α1KO mesangial cells would explain their excessive ROS production. Moreover, the fact that dominant negative Rac1 reduced ROS and collagen IV synthesis implied that Rac1 activation is upstream of ROS production.

We have clear evidence that the increase in collagen IV synthesis by α1KO mesangial cells is due, at least in part, to increased ROS production. Other cell types, including fibroblasts, can increase collagen in a ROS-dependent manner (50). In these cells, ROS contribute to the stabilization of H-Ras protein with subsequent ERK1/2-mediated collagen stimulation (50). Thus, as in fibroblasts, the ROS-dependent increased collagen production by α1KO mesangial cells may be due to activation of the Ras–mitogen-activated protein kinase pathway.

We found increased phosphorylation of the EGFR in α1KO mesangial cells. This observation agrees with the finding that integrin α1β1 negatively regulates EGFR signaling by activating the protein tyrosine phosphatase TCPTP (39). In this context, adhesion of integrin α1β1-expressing cells to collagen (thus engaging integrin α1β1) dramatically reduced EGF-induced EGFR phosphorylation, while persistent EGFR phosphorylation occurred in α1-deficient cells (39). Interestingly, although TCPTP was first described as a T-cell protein tyrosine phosphatase, this phosphatase is expressed in many different cell types (39), including primary mesangial cells (this study). Our observation that downregulation of TCPTP levels by siRNA in WT cells results in increased basal levels of phosphorylated EGFR strongly suggests that this tyrosine phos-

phatase is a key player in controlling integrin α1-dependent EGFR activation in mesangial cells.

In our model system, increased basal levels of phosphorylated EGFR were observed in α1KO cells relative to WT cells in the absence of EGF ligand. This increased phosphorylation may, in part, be due to constitutively high levels of ROS, which are known to initiate a number of physiological responses, including tyrosine phosphorylation of growth factor receptors such as platelet-derived growth factor receptor and EGFR (23). This possibility is strengthened by the observation that α1KO cells treated with antioxidants or transfected with N17Rac show decreased levels of phosphorylated EGFR. However, the fact that antioxidant-treated and/or N17Rac-expressing α1KO cells still show increased EGFR phosphorylation suggests that besides ROS, lack of integrin α1β1 per se also contributes to increased basal levels of EGFR phosphorylation in α1KO cells.

Treatment of cells with AG1478 decreased EGFR phosphorylation, Rac activation, and ROS synthesis. This observation suggests that in our model system the EGFR is required for Rac activation and agrees with the finding that EGFR activates Rac by phosphorylating and associating with Vav2, a Rac-GDP–GTP exchange factor (51). In addition, the effect of AG1478 on ROS productions agrees with the finding that glomerular fibrosis is ameliorated in vivo by treatment with the EGFR inhibitor gefitinib (12). The finding that AG1478 treatment completely inhibits the phosphorylation of Vav2 in cells transfected with TCPTP siRNA indicates that EGFR is the major, if not the only, activator of Vav2 in mesangial cells. These data stand in contrast to the finding that in adherent neutrophils, integrin engagement leads to inhibition of Vav1 activity via tyrosine phosphatase-mediated dephosphorylation of Tyr-174 of Vav1 (59). Thus, the Vav/Rac pathway may be regulated by growth factor receptors and/or tyrosine phosphatases.

Taken together, our data demonstrate that the increased collagen IV production by α1KO mesangial cells is due to the following cellular events. Lack of integrin α1β1 and recruitment of TCPTP result in increased EGFR activation, Vav2 phosphorylation, and Rac1 activation and translocation to the cell membrane (Fig. 11). This, in turn, results in increased ROS production, presumably by activation of the NADPH oxidase and increased collagen IV production (Fig. 11). In addition, ROS per se might induce increased EGFR phosphorylation, resulting in a positive feedback situation for increased collagen IV production (Fig. 11). In this context, ROS can inhibit the activity of tyrosine phosphatases by transient oxidation of thiol groups, with consequent formation of either an intramolecular S-S bridge or a sulfenyl-amide bond (5). Conversely, ROS-mediated oxidation of protein tyrosine kinases leads to their activation, either by direct SH modification or indirectly by concomitant inhibition of protein tyrosine phosphatases (5). The possibility that ROS might promote EGFR phosphorylation in our model is supported by the observation that α1KO cells treated with antioxidants (Fig. 7A) or expressing dominant negative Rac (Fig. 7B) show decreased levels of activated EGFR.

In conclusion, in addition to integrin α1β1 altering the phosphorylation status of the EGFR, the cross talk between this integrin and the EGFR also plays a key role in negatively modulating ROS and collagen IV production, which has major consequences in host responses to fibrosis-inducing stimuli.

ACKNOWLEDGMENTS

We are thankful to M. L. Tremblay for the generous gift of the anti-mouse TCPTP antibody.

This work was supported by R01-CA94849 (A.P.), R01-DK74359 (A.P.), O'Brien Center grant P50-DK39261-16 (A.P., R.Z., R.C.H.), RO1-DK69921 (R.Z.), RO1-DK54993 (D.B.P.), RO1-DK51265 (R.C.H.), and merit awards from the Department of Veterans Affairs (R.Z., R.C.H.).

REFERENCES

1. **Block, K., J. M. Ricono, D. Y. Lee, B. Bhandari, G. G. Choudhury, H. E. Abboud, and Y. Gorin.** 2006. Arachidonic acid-dependent activation of a $p22^{phox}$-based NAD(P)H oxidase mediates angiotensin II-induced mesangial cell protein synthesis and fibronectin expression via Akt/PKB. Antioxid. Redox Signal. **8:**1497–1508.
2. **Bokoch, G. M., and B. A. Diebold.** 2002. Current molecular models for NADPH oxidase regulation by Rac GTPase. Blood **100:**2692–2696.
3. **Bokoch, G. M., and T. Zhao.** 2006. Regulation of the phagocyte NADPH oxidase by Rac GTPase. Antioxid. Redox Signal. **8:**1533–1548.
4. **Chen, X., G. Moeckel, J. D. Morrow, D. Cosgrove, R. C. Harris, A. B. Fogo, R. Zent, and A. Pozzi.** 2004. Lack of integrin α1β1 leads to severe glomerulosclerosis after glomerular injury. Am. J. Pathol. **165:**617–630.
5. **Chiarugi, P.** 2005. PTPs versus PTKs: the redox side of the coin. Free Radic. Res. **39:**353–364.
6. **Corbetta, S., S. Gualdoni, C. Albertinazzi, S. Paris, L. Croci, G. G. Consalez, and I. de Curtis.** 2005. Generation and characterization of Rac3 knockout mice. Mol. Cell. Biol. **25:**5763–5776.
7. **Debidda, M., D. A. Williams, and Y. Zheng.** 2006. Rac1 GTPase regulates cell genomic stability and senescence. J. Biol. Chem. **281:**38519–38528.
8. **Defilippi, P., V. van Hinsbergh, A. Bertolotto, P. Rossino, L. Silengo, and G. Tarone.** 1991. Differential distribution and modulation of expression of α1/β1 integrin on human endothelial cells. J. Cell Biol. **114:**855–863.
9. **DeLeo, F. R., and M. T. Quinn.** 1996. Assembly of the phagocyte NADPH oxidase: molecular interaction of oxidase proteins. J. Leukoc. Biol. **60:**677–691.
10. **del Pozo, M. A., N. B. Alderson, W. B. Kiosses, H. H. Chiang, R. G. Anderson, and M. A. Schwartz.** 2004. Integrins regulate Rac targeting by internalization of membrane domains. Science **303:**839–842.
11. **del Pozo, M. A., L. S. Price, N. B. Alderson, X. D. Ren, and M. A. Schwartz.** 2000. Adhesion to the extracellular matrix regulates the coupling of the small GTPase Rac to its effector PAK. EMBO J. **19:**2008–2014.
12. **Francois, H., S. Placier, M. Flamant, P. L. Tharaux, D. Chansel, J. C. Dussaule, and C. Chatziantoniou.** 2004. Prevention of renal vascular and glomerular fibrosis by epidermal growth factor receptor inhibition. FASEB J. **18:**926–928.
13. **Gandhi, P. N., R. M. Gibson, X. Tong, J. Miyoshi, Y. Takai, M. Konieczkowski, J. R. Sedor, and A. L. Wilson-Delfosse.** 2004. An activating mutant of Rac1 that fails to interact with Rho GDP-dissociation inhibitor stimulates membrane ruffling in mammalian cells. Biochem. J. **378:**409–419.
14. **Gardner, H., A. Broberg, A. Pozzi, M. Laato, and J. Heino.** 1999. Absence of integrin α1β1 in the mouse causes loss of feedback regulation of collagen synthesis in normal and wounded dermis. J. Cell Sci. **112:**263–272.
15. **Gardner, H., J. Kreidberg, V. Koteliansky, and R. Jaenisch.** 1996. Deletion of integrin α1 by homologous recombination permits normal murine development but gives rise to a specific deficit in cell adhesion. Dev. Biol. **175:**301–313.
16. **Geiszt, M., J. B. Kopp, P. Varnai, and T. L. Leto.** 2000. Identification of renox, an NAD(P)H oxidase in kidney. Proc. Natl. Acad. Sci. USA **97:**8010–8014.
17. **Glaven, J. A., I. Whitehead, S. Bagrodia, R. Kay, and R. A. Cerione.** 1999. The Dbl-related protein, Lfc, localizes to microtubules and mediates the activation of Rac signaling pathways in cells. J. Biol. Chem. **274:**2279–2285.
18. **Glogauer, M., C. C. Marchal, F. Zhu, A. Worku, B. E. Clausen, I. Foerster, P. Marks, G. P. Downey, M. Dinauer, and D. J. Kwiatkowski.** 2003. Rac1 deletion in mouse neutrophils has selective effects on neutrophil functions. J. Immunol. **170:**5652–5657.
19. **Gorin, Y., J. M. Ricono, N. H. Kim, B. Bhandari, G. G. Choudhury, and H. E. Abboud.** 2003. Nox4 mediates angiotensin II-induced activation of Akt/protein kinase B in mesangial cells. Am. J. Physiol. Renal Physiol. **285:**F219–F229.
20. **Gu, Y., B. Jia, F. C. Yang, M. D'Souza, C. E. Harris, C. W. Derrow, Y. Zheng, and D. A. Williams.** 2001. Biochemical and biological characterization of a human Rac2 GTPase mutant associated with phagocytic immunodeficiency. J. Biol. Chem. **276:**15929–15938.
21. **Honore, S., H. Kovacic, V. Pichard, C. Briand, and J. B. Rognoni.** 2003.

$\alpha 2\beta 1$-integrin signaling by itself controls G_1/S transition in a human adenocarcinoma cell line (Caco-2): implication of NADPH oxidase-dependent production of ROS. Exp. Cell Res. **285:**59–71.
22. **Hordijk, P. L.** 2006. Regulation of NADPH oxidases: the role of Rac proteins. Circ. Res. **98:**453–462.
23. **Huang, R. P., J. X. Wu, Y. Fan, and E. D. Adamson.** 1996. UV activates growth factor receptors via reactive oxygen intermediates. J. Cell Biol. **133:** 211–220.
24. **Ibarra-Sanchez, M. J., J. Wagner, M. T. Ong, C. Lampron, and M. L. Tremblay.** 2001. Murine embryonic fibroblasts lacking TC-PTP display delayed G_1 phase through defective NF-κB activation. Oncogene **20:**4728–4739.
25. **Inoguchi, T., H. Tsubouchi, T. Etoh, M. Kakimoto, T. Sonta, H. Utsumi, H. Sumimoto, H. Y. Yu, N. Sonoda, M. Inuo, N. Sato, N. Sekiguchi, K. Kobayashi, and H. Nawata.** 2003. A possible target of antioxidative therapy for diabetic vascular complications—vascular NAD(P)H oxidase. Curr. Med. Chem. **10:**1759–1764.
26. **Jones, S. A., J. T. Hancock, O. T. Jones, A. Neubauer, and N. Topley.** 1995. The expression of NADPH oxidase components in human glomerular mesangial cells: detection of protein and mRNA for $p47^{phox}$, $p67^{phox}$, and $p22^{phox}$. J. Am. Soc. Nephrol. **5:**1483–1491.
27. **Kheradmand, F., E. Werner, P. Tremble, M. Symons, and Z. Werb.** 1998. Role of Rac1 and oxygen radicals in collagenase-1 expression induced by cell shape change. Science **280:**898–902.
28. **Kim, C., and M. C. Dinauer.** 2001. Rac2 is an essential regulator of neutrophil nicotinamide adenine dinucleotide phosphate oxidase activation in response to specific signaling pathways. J. Immunol. **166:**1223–1232.
29. **Kitagawa, Y., M. Ueda, N. Ando, S. Ozawa, and M. Kitajima.** 1995. Effect of endogenous and exogenous EGF on the growth of EGF receptor-hyperproducing human squamous cell carcinoma implanted in nude mice. Br. J. Cancer **72:**865–868.
30. **Korhonen, M., J. Ylanne, L. Laitinen, and I. Virtanen.** 1990. The $\alpha 1$-$\alpha 6$ subunits of integrins are characteristically expressed in distinct segments of developing and adult human nephron. J. Cell Biol. **111:**1245–1254.
31. **Kurokawa, K., R. E. Itoh, H. Yoshizaki, Y. O. Nakamura, and M. Matsuda.** 2004. Coactivation of Rac1 and Cdc42 at lamellipodia and membrane ruffles induced by epidermal growth factor. Mol. Biol. Cell **15:**1003–1010.
32. **Kwan, J., H. Wang, S. Munk, L. Xia, H. J. Goldberg, and C. I. Whiteside.** 2005. In high glucose protein kinase C-ζ activation is required for mesangial cell generation of reactive oxygen species. Kidney Int. **68:**2526–2541.
33. **Lakhe-Reddy, S., S. Khan, M. Konieczkowski, G. Jarad, K. L. Wu, L. F. Reichardt, Y. Takai, L. A. Bruggeman, B. Wang, J. R. Sedor, and J. R. Schelling.** 2006. β8 integrin binds Rho GDP dissociation inhibitor-1 and activates Rac1 to inhibit mesangial cell myofibroblast differentiation. J. Biol. Chem. **281:**19688–19699.
34. **Lassegue, B., and R. E. Clempus.** 2003. Vascular NAD(P)H oxidases: specific features, expression, and regulation. Am. J. Physiol. Regul. Integr. Comp. Physiol. **285:**R277–R297.
35. **Lee, E. A., J. Y. Seo, Z. Jiang, M. R. Yu, M. K. Kwon, H. Ha, and H. B. Lee.** 2005. Reactive oxygen species mediate high glucose-induced plasminogen activator inhibitor-1 up-regulation in mesangial cells and in diabetic kidney. Kidney Int. **67:**1762–1771.
36. **Leung, K., A. Nagy, I. Gonzalez-Gomez, J. Groffen, N. Heisterkamp, and V. Kaartinen.** 2003. Targeted expression of activated Rac3 in mammary epithelium leads to defective postlactational involution and benign mammary gland lesions. Cells Tissues Organs **175:**72–83.
37. **Li, J. M., and A. M. Shah.** 2003. ROS generation by nonphagocytic NADPH oxidase: potential relevance in diabetic nephropathy. J. Am. Soc. Nephrol. **14:**S221–S226.
38. **Marcoux, N., and K. Vuori.** 2003. EGF receptor mediates adhesion-dependent activation of the Rac GTPase: a role for phosphatidylinositol 3-kinase and Vav2. Oncogene **22:**6100–6106.
39. **Mattila, E., T. Pellinen, J. Nevo, K. Vuoriluoto, A. Arjonen, and J. Ivaska.** 2005. Negative regulation of EGFR signalling through integrin-$\alpha 1\beta 1$-mediated activation of protein tyrosine phosphatase TCPTP. Nat. Cell Biol. **7:**78–85.
40. **Miyata, K., M. Rahman, T. Shokoji, Y. Nagai, G. X. Zhang, G. P. Sun, S. Kimura, T. Yukimura, H. Kiyomoto, M. Kohno, Y. Abe, and A. Nishiyama.** 2005. Aldosterone stimulates reactive oxygen species production through activation of NADPH oxidase in rat mesangial cells. J. Am. Soc. Nephrol. **16:**2906–2912.
41. **Nobes, C. D., and A. Hall.** 1999. Rho GTPases control polarity, protrusion, and adhesion during cell movement. J. Cell Biol. **144:**1235–1244.
42. **Pankov, R., Y. Endo, S. Even-Ram, M. Araki, K. Clark, E. Cukierman, K. Matsumoto, and K. M. Yamada.** 2005. A Rac switch regulates random versus directionally persistent cell migration. J. Cell Biol. **170:**793–802.
43. **Pozzi, A., S. Coffa, N. Bulus, W. Zhu, D. Chen, X. Chen, G. Mernaugh, Y. Su, S. Cai, A. Singh, M. Brissova, and R. Zent.** 2006. H-Ras, R-Ras and TC21 differentially regulate ureteric bud cell branching morphogenesis. Mol. Biol. Cell **17:**2046–2056.
44. **Pozzi, A., P. E. Moberg, L. A. Miles, S. Wagner, P. Soloway, and H. A. Gardner.** 2000. Elevated matrix metalloprotease and angiostatin levels in integrin $\alpha 1$ knockout mice cause reduced tumor vascularization. Proc. Natl. Acad. Sci. USA **97:**2202–2207.
45. **Pozzi, A., K. K. Wary, F. G. Giancotti, and H. A. Gardner.** 1998. Integrin $\alpha 1\beta 1$ mediates a unique collagen-dependent proliferation pathway in vivo. J. Cell Biol. **142:**587–594.
46. **Radhakrishna, H., O. Al-Awar, Z. Khachikian, and J. G. Donaldson.** 1999. ARF6 requirement for Rac ruffling suggests a role for membrane trafficking in cortical actin rearrangements. J. Cell Sci. **112**(Pt. 6)**:**855–866.
47. **Segal, A. W., and A. Abo.** 1993. The biochemical basis of the NADPH oxidase of phagocytes. Trends Biochem. Sci. **18:**43–47.
48. **Shiose, A., J. Kuroda, K. Tsuruya, M. Hirai, H. Hirakata, S. Naito, M. Hattori, Y. Sakaki, and H. Sumimoto.** 2001. A novel superoxide-producing NAD(P)H oxidase in kidney. J. Biol. Chem. **276:**1417–1423.
49. **Suzuki-Inoue, K., Y. Yatomi, N. Asazuma, M. Kainoh, T. Tanaka, K. Satoh, and Y. Ozaki.** 2001. Rac, a small guanosine triphosphate-binding protein, and p21-activated kinase are activated during platelet spreading on collagen-coated surfaces: roles of integrin $\alpha_2\beta_1$. Blood **98:**3708–3716.
50. **Svegliati, S., R. Cancello, P. Sambo, M. Luchetti, P. Paroncini, G. Orlandini, G. Discepoli, R. Paterno, M. Santillo, C. Cuozzo, S. Cassano, E. V. Avvedimento, and A. Gabrielli.** 2005. Platelet-derived growth factor and reactive oxygen species (ROS) regulate Ras protein levels in primary human fibroblasts via ERK1/2. Amplification of ROS and Ras in systemic sclerosis fibroblasts. J. Biol. Chem. **280:**36474–36482.
51. **Tamas, P., Z. Solti, P. Bauer, A. Illes, S. Sipeki, A. Bauer, A. Farago, J. Downward, and L. Buday.** 2003. Mechanism of epidermal growth factor regulation of Vav2, a guanine nucleotide exchange factor for Rac. J. Biol. Chem. **278:**5163–5171.
52. **Tzima, E., M. A. Del Pozo, W. B. Kiosses, S. A. Mohamed, S. Li, S. Chien, and M. A. Schwartz.** 2002. Activation of Rac1 by shear stress in endothelial cells mediates both cytoskeletal reorganization and effects on gene expression. EMBO J. **21:**6791–6800.
53. **Voigt, S., R. Gossrau, O. Baum, K. Loster, W. Hofmann, and W. Reutter.** 1995. Distribution and quantification of $\alpha 1$-integrin subunit in rat organs. Histochem. J. **27:**123–132.
54. **Werner, E., and Z. Werb.** 2002. Integrins engage mitochondrial function for signal transduction by a mechanism dependent on Rho GTPases. J. Cell Biol. **158:**357–368.
55. **Xia, L., H. Wang, H. J. Goldberg, S. Munk, I. G. Fantus, and C. I. Whiteside.** 2006. Mesangial cell NADPH oxidase upregulation in high glucose is protein kinase C dependent and required for collagen IV expression. Am. J. Physiol. Renal Physiol. **290:**F345–F356.
56. **Zaidel-Bar, R., C. Ballestrem, Z. Kam, and B. Geiger.** 2003. Early molecular events in the assembly of matrix adhesions at the leading edge of migrating cells. J. Cell Sci. **116:**4605–4613.
57. **Zent, R., C. A. Fenczik, D. A. Calderwood, S. Liu, M. Dellos, and M. H. Ginsberg.** 2000. Class- and splice variant-specific association of CD98 with integrin beta cytoplasmic domains. J. Biol. Chem. **275:**5059–5064.
58. **Zent, R., X. Yan, Y. Su, B. G. Hudson, D. B. Borza, G. W. Moeckel, Z. Qi, Y. Sado, M. D. Breyer, P. Voziyan, and A. Pozzi.** 2006. Glomerular injury is exacerbated in diabetic integrin $\alpha 1$-null mice. Kidney Int. **70:**460–470.
59. **Zhao, T., V. Benard, B. P. Bohl, and G. M. Bokoch.** 2003. The molecular basis for adhesion-mediated suppression of reactive oxygen species generation by human neutrophils. J. Clin. Investig. **112:**1732–1740.